Green Chemistry

PAPER

Cite this: *Green Chem.*, 2022, **24**, 916

Sustainable NO_x production from air in pulsed plasma: elucidating the chemistry behind the low energy consumption†

Elise Vervloessem, *[a,b] Yury Gorbanev, [a] Anton Nikiforov,[b] Nathalie De Geyter[b] and Annemie Bogaerts [a]

Received 2nd August 2021,
Accepted 21st December 2021

DOI: 10.1039/d1gc02762j

rsc.li/greenchem

N-Based fertilisers are paramount to support our still-growing world population. Current industrial N_2 fixation is heavily fossil fuel-dependent, therefore, a lot of work is put into the development of fossil-free pathways. Plasma technology offers a fossil-free and flexible method for N_2 fixation that is compatible with renewable energy sources. We present here a pulsed plasma jet for direct NO_x production from air. The pulsed power allows for a record-low energy consumption (EC) of 0.42 MJ (mol N)$^{-1}$. This is the lowest reported EC in plasma-based N_2 fixation at atmospheric pressure thus far. We compare our experimental data with plasma chemistry modelling, and obtain very good agreement. Hence, we can use our model to explain the underlying mechanisms responsible for this low EC. The pulsed power and the corresponding pulsed gas temperature are the reason for the very low EC: they provide a strong vibrational–translational non-equilibrium and promote the non-thermal Zeldovich mechanism. This insight is important for the development of the next generation of plasma sources for energy-efficient NO_x production.

Introduction

Transforming atmospheric, chemically inert N_2 into reactive, or accessible, nitrogen (N_2 fixation) is a crucial step in producing fertilisers for the world-wide agricultural sector. Though nature provides fixated N_2 *via* microorganism activity, the ever-growing world population demands more fixed N_2 than the earth can naturally provide. About 232 million tonnes of fixed N_2 would be needed per year by 2050, as projected by Bodirsky *et al.*[1] To compare, biological N_2 fixation is estimated to fix 100–175 million tonnes of N_2 per year.[2]

Over the past century, fertilisers and base chemicals like ammonia (NH_3) have been avidly produced synthetically to make up for the high demand. Currently 50% of the world's population depends on the production of said fixed N_2 in the form of NH_3 through the Haber–Bosch (HB) process.[3] While this process plays a crucial role in food and base chemical production, it consumes 1.8% of the world's energy supply[4] and relies on fossil fuels (natural gas) both as energy provider and source of H_2.[5] Thus, while a synthetic N_2 fixation process is necessary, the current industrial HB process does not fit into the concept of sustainable production.

Due to its great economic importance, the HB process has been extensively optimised over the last 100 years and is currently the most energy-efficient process for NH_3 synthesis. There are no easy reductions in energy consumption left; bettering the way N_2 is fixed requires drastic changes in the technology as well as process innovation.

Noteworthily, currently the commercial production of activated N_2 chemicals predominantly uses the NH_3 produced by the HB process as a basis. For example, nitric acid (HNO_3), one of the main constituents of nitrogen-based and some potassium-based fertilisers and one of the world's 15 largest commodity chemicals,[6] is commercially produced *via* the Ostwald process, which converts NH_3 into HNO_3 in two steps *via* NO_x[7] (Fig. 1). The production of HNO_3 is therefore directly limited by NH_3 production through the HB process. This is why half of the world's population depends on one single chemical process.

Naturally, there is a growing interest in alternative or complementary processes for N_2 fixation, such as enzyme-based, plasma-based, and (electro)catalytic methods with both heterogeneous and homogeneous catalysts.[8,9] Among the different techniques mentioned, plasma-based N_2 fixation is particularly appealing because of its flexibility and synergy with sustainable energy sources.[8,10–13]

Plasma is most commonly produced by applying an electric field to a gas, causing gas breakdown, resulting in the production of a range of reactive species, including electrons, ions, radicals, excited species and photons.[10] Fig. 1 shows the

[a]*University of Antwerp, Universiteitsplein 1, 2610 Antwerp, Belgium.*
E-mail: elise.vervloessem@uantwerpen.be, annemie.bogaerts@uantwerpen.be
[b]*Ghent University, Sint-Pietersnieuwstraat 25, 9000 Ghent, Belgium*

†Electronic supplementary information (ESI) available. See DOI: 10.1039/d1gc02762j

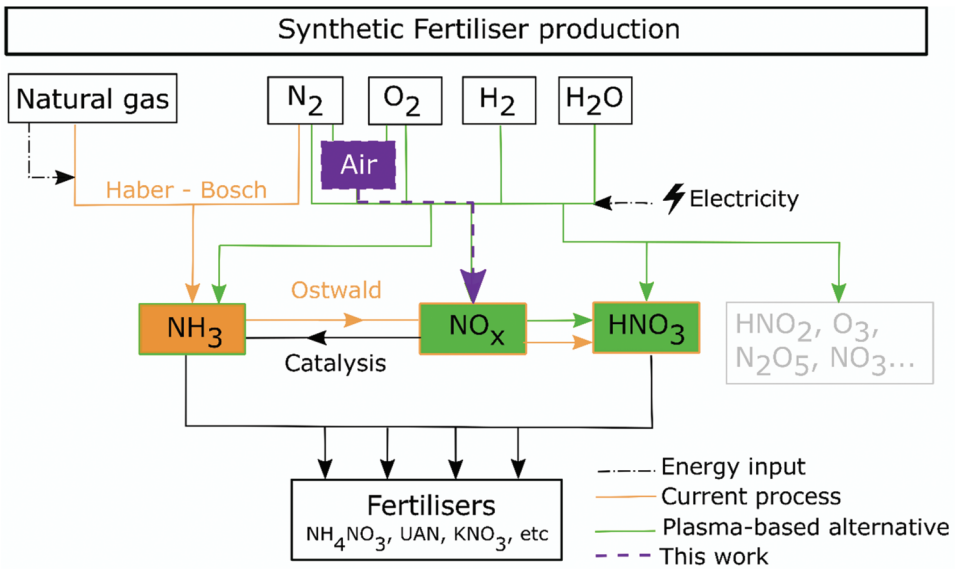

Fig. 1 Scheme of the current and plasma-based alternative routes for the production of synthetic fertilisers. The orange lines show the current route (Haber–Bosch + Ostwald), the green lines show the plasma-based processes with a variety of feed gas combinations. The black dash-dotted lines show the main energy source for both processes, *i.e.*, fossil fuel-based on the left (natural gas) and electricity-based on the right. The dashed purple line indicates the subject of this work. UAN is a urea and NH_4NO_3 (ammonium nitrate) based fertiliser.

different types of plasma-based N_2 fixation pathways into NO_x and NH_3 by means of different $N_2/O_2/H_2O/H_2$ gas combinations: (1) NO_x can be formed in plasma from an N_2/O_2 feed gas in different ratios,[14,15] of which the most accessible is air, but it can also be formed in other common N_2/H_2O and $N_2/O_2/H_2O$ combinations, like air[16] and N_2 containing water vapour.[17] Note that NO_x can be used directly in the production of HNO_3[11] (see above) or can be reduced post-plasma for the production of NH_3.[12] (2) NH_3 is mostly produced in plasma from N_2/H_2 using catalysts,[13] but can also be formed *via* plasma treatment of humid (*i.e.*, water vapour-containing) air,[16] humid N_2 or $N_2/O_2/H_2O/H_2$ in other ratios.[17] Recent reports also describe N_2 fixation into N-doped quantum dots.[18]

Using plasma tackles a major problem of the current industrial HB process. Indeed, despite major efforts to electrify the HB process,[13] it is still mainly fossil fuel dependent, inflexible, and only truly energy-efficient at a large scale. Plasma-based processes, on the other hand, are electricity-based, flexible, and can operate on a small scale for decentralisation.[11] The mentioned flexibility implies that plasmas are easily turned on/off (turnkey process). The fact that plasmas only need electricity as the energy source combines well with renewable (*e.g.* solar) electricity, by providing peak shaving and grid stabilisation.[10] Additionally, small scale plasma reactors can produce fertilisers on the sites where they are needed, reducing transport costs together with increasing availability of fertilisers in remote areas.[19] Thus, a commercial plasma-based N_2 fixation process would imply a green and energy-efficient fertiliser and base chemicals production that is: (1) carbon-neutral, and (2) compatible with renewable energy sources. The first plasma-based N_2 fixation process was introduced in the beginning of the 20th century by Birkeland and Eyde, who converted air into NO through a thermal arc furnace (1–2% yield at an energy consumption (EC) of 2.41 MJ (mol N)$^{-1}$).[20] More than a century later, a wide range of plasma types have been studied for plasma-based NO_x production, driven by the need for an alternative to the current industrial process, including thermal plasmas,[20,21] spark discharges,[22,23] radio-frequency discharges,[24] laser-produced discharges,[25] corona discharges,[22,26] glow discharges,[27,28] (packed bed) dielectric barrier discharges,[27,29] microwave discharges,[30–34] different types of arc discharges[14,15,19,27,35–37] (including pulsed arc and gliding arc) and plasma jets in contact with water.[26,38] An overview of the reported EC and product concentrations is given in the Results and discussion section. The NO_x concentration is generally in the 1% range (0.1–14.0%), while the EC spans over a very large range (0.28–1673 MJ (mol N)$^{-1}$). Important to note, the best performance values apply to low-pressure plasma reactors, and did not account for the energy required to maintain low pressure and cooling of the reactor; moreover, these values (1980s)[33] have not been reproduced since then. In general, to the best of our knowledge, the theoretical minimum EC for plasma-based NO_x production (0.2 MJ (mol N)$^{-1}$) has not yet been reached. The best values reported for atmospheric-pressure plasmas apply to gliding arc reactors (2.4–3.6 MJ (mol N)$^{-1}$).[14,15,19,36,37,39] and recently, record values of 2 MJ (mol N)$^{-1}$ have been reported by Kelly and Bogaerts in an atmospheric pressure MW plasma.[34]

A number of literature reports discuss the underlying chemical mechanisms, either purely experimental[26] or supported by modelling.[14,15,36,37] It is generally known that the most energy-efficient pathway to NO_x is *via* the non-thermal Zeldovich mechanism promoted by vibrational

excitation.[10,11,14,15,26,36] (Reactions (R1) and (R2); where g and v stand for the ground state and the vibrationally excited states of the molecule, respectively. The mechanism (R1 and R2) inherently includes the thermal Zeldovich mechanism.)

$$O_2(v,g) + N \rightarrow NO + O \quad (R1)$$

$$N_2(v,g) + O \rightarrow NO + N \quad (R2)$$

Vibrationally excited molecules decrease the activation energy barrier, facilitating the reaction.[10] The Zeldovich mechanism can thus be exploited by overpopulation of the vibrational levels. A so-called "vibrational–translational (V–T) non-equilibrium" can be induced through pulsing[27,40] and low values of the reduced electric field.[36] Exploiting the non-thermal Zeldovich mechanism to achieve the theoretical minimum EC in practice is one of the holy grails in plasma-based NO_x production research. Furthermore, besides the direct formation of NO_x, minimising its destruction *via* back reactions and maximising the fraction of gas treated by the plasma are two common challenges in this research field.[11,14,15]

In this work, we present a combined computational and experimental study of a pulsed plasma jet operating in air – the so-called Soft Jet.[41,42] The pulsing plasma (*i.e.*, plasma with pulsed power) is attractive because pulsing helps to reach V–T non-equilibrium at atmospheric pressure,[40,43,44] required to achieve the theoretical minimum EC for plasma-based NO_x production of 0.2 MJ (mol N)$^{-1}$.[45,46] To date, no dedicated study – neither experimental nor computational – has been performed to elucidate the underlying mechanisms of NO_x formation induced by pulsing plasmas in dry air.

We show that our Soft Jet plasma exhibits a very low EC (*ca.* 0.42 MJ (mol N)$^{-1}$) for NO_x production, and we try to elucidate the underlying mechanisms, by experiments and modelling, to gain insight into the role of pulsing in the plasma chemistry, and consequently its effect on this low EC. The aim of our work is to address the applicability of plasma technology, by discussing how detailed insights in the underlying mechanisms can be used to improve the NO_x yield and EC in plasma-based N_2 fixation.

Experimental

Plasma setup

A photograph of the Soft Jet is presented in Fig. 2a, and schematically shown in Fig. 2b. A powered needle is ringed by a tipped quartz capillary (outer diameter 5 mm and inner diameter 2 mm, at the widest part) and contained in a metal tube. A metal nozzle is screwed on the top and acts as the ground electrode and outlet of the jet (outlet diameter 1.2 mm). The quartz in between the inlet gas and the metal tube acts as a dielectric spacer (see Fig. 2b). The feed gas is supplied through the quartz capillary and leaves the jet *via* the nozzle tip. Compressed dry air (Air Liquide Alphagaz 1, purity ≥ 99.999%) is introduced into the Soft Jet. The gas flow rates are controlled by a Bronkhorst EL-FLOW® F-201CV mass flow controller (MFC) and range from 0.4 to 2.0 L min^{-1}.

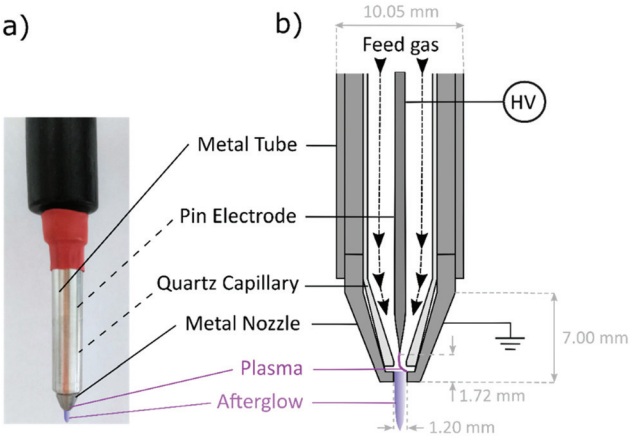

Fig. 2 (a) Side view of the Soft Jet. The dashed lines indicate parts that are located on the inside. The plasma effluent (afterglow) is manually drawn in purple as it would not be clearly visible in a picture. (b) Schematic of the inside of the Soft Jet, with some dimensions. The dashed arrow lines indicate the gas flow direction through the jet.

Voltage–current (*V–I*) waveforms and plasma power

The voltage–current (*V–I*) waveform of the Soft Jet is plotted in the ESI; Fig. S.1.† On a large time scale (Fig. S.1a†) the Soft Jet produces short (26.3 ms) sequences of pulses ("pulse trains") with a longer pulse-off time in between (149.9 ms). One pulse train consists of 4420 pulses with the current and voltage characteristics shown in Fig. S.1b and c.† As demonstrated in our previous work,[17] the current and voltage waveforms during a pulse train are close to sinusoidal in shape[17] (Fig. S.1c†). The discharge mechanism is similar to a low current spark operating in a pulsed mode.[17,47] Through emission spectroscopy, it was observed that plasma emission is only detected during the small peaks in the *V–I* waveform, which means the plasma is only formed for a short duration (0.74 μs) during the small *V–I* peaks. This is confirmed by the lack of optical emission (radiation) by the plasma-generated species during the interpulse time (5.21 μs).[17] Fig. S.1† shows two representative ICCD images, *i.e.*, (I) during the pulse and (II) during the interpulse, to support this. The measured power of one pulse (5.11 W, *i.e.* the power reached during a pulse; see Section S.1† for detailed description of the calculation) does not equal the power put into the system. Indeed, there is a pulse train only during 14.9% of the time, and within this pulse train there is only a pulse during 12.4% of the time. Hence, the total duty cycle of the Soft Jet is merely 1.9% (12.4% × 14.9%), meaning the plasma power consumption of the Soft Jet is only 0.1 W.[17]

We note that the power used for the calculation of the EC refers to the plasma power, which does not equal the applied power but the part of the total power directly dissipated during the plasma pulse. The remaining power was not accounted for in the EC calculation. This approach is custom in plasma research,[48,49] where the focus is on the efficiency and characteristics of the plasma itself, as opposed to the optimization of the power source which is a field on its own. Details on this

plasma power measurement can be found in ESI, Section S.1.† Henceforth, the term power will always refer to plasma power.

For clarification: there exist several viewpoints for the power calculation. Depending on the engineering purpose, the power can be defined as electrical power of the wall plug, power delivered to the reactor, or power absorbed in the plasma (Fig. S.2†). The exact methodology of power calculations is therefore in many ways defined by the application. In this work, and many other plasma chemistry works, the focus is on the chemical efficiency of the plasma, *i.e.* the power consumed during the plasma pulses, is used for energy cost calculation, while the total wall plug power is not considered. We acknowledge that optimising the electrical features of the plasma setup is an important task, but it lies outside the immediate scope of our work.

Our experiments revealed that the waveforms and other plasma ignition parameters are virtually independent of the gas composition for N_2, humid N_2, air and humid air.[17] Therefore, here we apply our previous results of the diagnostics obtained in N_2 and humid N_2, for the dry air plasma used in our current work. The detailed diagnostics of the Soft Jet are found elsewhere.[17]

Analysis of the plasma-treated gas

The plasma-treated gas (consisting of the products and unconverted feed gas) was analysed by Fourier-transform infrared spectroscopy (FTIR) using a Matrix-MG2 Bruker FTIR spectrometer, enabling the quantitative analysis of the concentrations of NO, NO_2, N_2O_5, N_2O, and ozone. The optical path length inside the gas cell was 5.0 m and the absolute calibrations were performed by Bruker. Spectra were obtained with an average of 50 scans with a resolution of 0.5 cm^{-1}.

The experiments were performed in triplicates for each flow rate and the average was taken over a 15 min measurement period chosen to stabilise the FTIR measurements. The system was flushed thoroughly with air for at least 15 min in between measurements. The reported concentrations and error bars are the weighted average of this set of three measurements.

Energy consumption (EC) calculation

Using the plasma power (P) and the total NO_x concentration, the EC was calculated according to eqn (1). The EC is expressed in MJ (mol N)$^{-1}$, where mol N is the amount of nitrogen fixed.

$$\mathrm{EC}\,[\mathrm{MJ\,mol^{-1}\,N^{-1}}] = \frac{P\,[W]}{\text{mol of } NO_x \text{ produced per second } [\mathrm{mol\,s^{-1}}]} \cdot \frac{1}{10^6\,[\mathrm{J\,MJ^{-1}}]} \quad (1)$$

Model description

Quasi-1D plasma chemical kinetics model

To gain insight into the gas phase chemistry taking place in the Soft Jet, we developed a quasi-1D chemical kinetics model within the Zero-Dimensional (0D) Plasma Kinetics solver, ZDPlasKin.[50] The model calculates among others the NO_x concentration and reveals the underlying mechanisms. The densities of the various plasma species are obtained as a function of time by numerically solving the continuity equation (see Section S.2.1 in the ESI†) for each species included in the model (Table 1), taking into account the production and loss terms by the chemical reactions. This type of modelling allows to describe an extensive chemistry without extreme computational load. To account for spatial variations, the time dependence of the model ("batch reactor") is transformed into a spatial dependence ("plug flow reactor") using a gas velocity profile through the Soft Jet, as explained in Section S.2.2 of the ESI.† This velocity profile is determined by CFD calculations (Section S.2.3 of the ESI†). The plasma characteristics thus vary as a function of the distance travelled by the gas through the Soft Jet. In essence, this transforms the time-dependent 0D model into a quasi-1D model. More detailed information on the model and the equations can be found in the ESI (Section S.2†).

The quasi-1D model starts with a plasma zone, wherein the molecules experience the pulse train. The number of pulses depends on the gas flow rate, and thus the residence time in the plasma: a longer residence time means the gas encounters more pulses (320 pulses at a gas flow rate of 0.1 L min^{-1}; 15 pulses at 2.0 L min^{-1}). The gas temperature profile and the power profile as a function of time, as experienced by the molecules, were used as input in the model to simulate the pulses, and are plotted in Fig. 3a. Details on how they were

Table 1 Species included in the model

N_2 species	
Neutral ground state molecules and atoms	N_2, N
Ions	N^+, N_2^+, N_3^+, N_4^+
Vibrationally excited molecules	$N_2(v_1 - v_{24})$
Electronically excited molecules or atoms	$N_2(A^3\sum_u^+)$, $N_2(B^3\prod_g)$, $N_2(C^3\prod_u)$ and $N_2(a'^1\sum_u^-)$, N(2D), N(2P)
N_xO_y species	
NO, N_2O, NO_2, NO_3, N_2O_5, N_2O_3, N_2O_4, NO^+, N_2O^+, NO_2^+, NO^-, N_2O^-, NO_2^-, NO_3^-, $N_2O_2^+$	
O_2 species	
Neutral ground state molecules and atoms	O_2, O_3, O
Ions	O^-, O_2^-, O_3^-, O_4^-, O^+, O_2^+, O_4^+
Vibrationally excited molecules	$O_2(v_1 - v_{15})$
Electronically excited molecules or atoms	O(1D), O(1S), $O_2(a^1\Delta)$, $O_2(b^1\sum^+)$ and a combination of three states, *i.e.* $O_2(A^3\sum^+, C^3\Delta, c^1\sum^-)$ at a threshold energy of 4.5 eV.

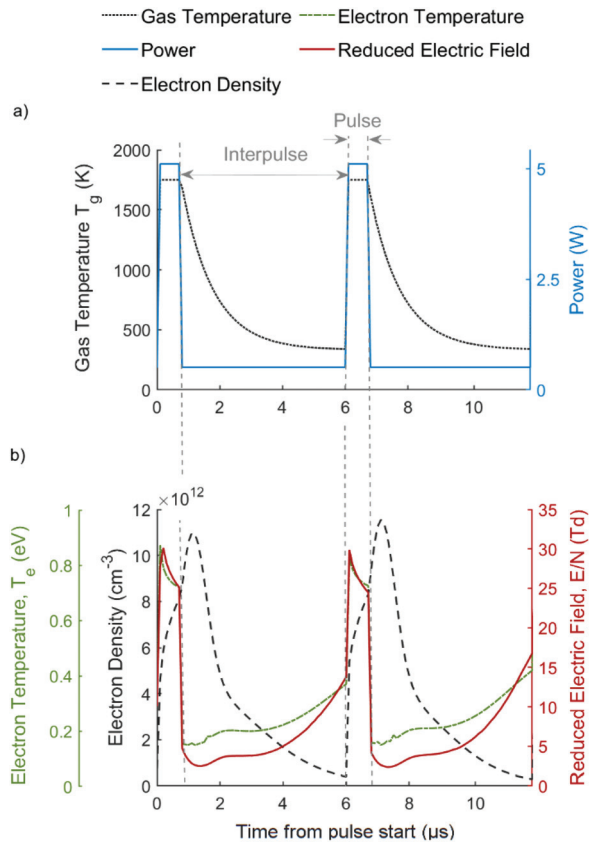

Fig. 3 (a) Input plasma parameters in the model, *i.e.,* gas temperature and power for two pulses. (b) Calculated plasma characteristics, *i.e.,* electron temperature, electron density and reduced electric field, as calculated in the model, for air composition (80/20 N_2/O_2) and feed gas flow rate 1 L min^{-1}. The vertical grey dashed lines indicate the pulse and interpulse times.

deduced from the voltage waveform, experiments are provided in the ESI (Section S.2.2.2†). In short, the power deposited in the plasma, considering that the plasma is only formed during the peak (= one pulse) of the voltage-waveform corresponds to 5.11 W for the duration of the pulse. In between the pulses (*i.e.* the so-called interpulse period), the power was set to 10% of the peak power (details in ESI: Sections S.2.2.2a and c†).

The gas temperature profile in the plasma is based on optical emission spectroscopy (OES) measurements by a line of sight looking straight into the Soft Jet and is virtually independent of flow rate, as reported in our recent work.[17] We chose OES as the only way to measure the discharge temperature, due to the geometric constraints. OES is a well-established technique for monitoring the plasma temperature,[51–54] and the spectral band used is representative for the gas temperature under the conditions of our experiments.[52] We refer to our previous works for a detailed description of the OES methodology. The temperature during the pulses, *i.e.* the gas temperature of the plasma arc is 1750 ± 150 K. This was found to be the same within the error margin (*ca.* 150 K), for the entire range of flow rates investigated (0.2–2 L min^{-1}). There are a variety of processes including heat exchange, arc elongation, possible arc constriction and even rotation that could result in a change of gas temperature of the plasma as the flow changes. Based on the OES measurements, we can conclude that these processes are not dominant, or counteract each other, and therefore do not influence the gas temperature of the plasma to a degree which would be experimentally observable. One possible explanation is as follows: the constant gas temperature is representative of the fact that there are a number of mechanisms of gas heating at play. Indeed, as the flow rate increases, the arc compresses but also elongates, resulting in a constant energy deposition in the arc. The arc elongation does not significantly increase the voltage due to the low power dissipation and low resistivity of the discharge. Note, the change in flow could result in other more elaborate changes in arc dynamics, such as rotation, which influences the heat transfer as well. The full detailed study of the arc dynamics would require either full-scale 3D modelling or direct optical access to the arc region which is not possible in the current configuration of the plasma reactor. As the interpulse gas temperature could not be measured directly due to the small time scale of the pulses, the gas temperature during the interpulse period was set to an exponential decay to 330 K in accordance with the average gas temperature measured by Rayleigh scattering in the afterglow[17] This approximation was found valid through a sensitivity test described in ESI, Section S.2.2.2b.† (See Fig. 3a, and details in ESI: Section S.2.2.2b and Fig. S.5.†)

The plasma zone with the pulse train is followed by an afterglow, *i.e.* outside of the jet nozzle, where post-plasma reactions can take place. In this region, the power was set to zero and the gas temperature profile for each flow rate was calculated based on Rayleigh-gas temperature measurements by a line of sight perpendicular to the Soft Jet.[17] In reality, the temperature decrease in the afterglow is flow rate dependent and likely due to the change of heat transfer at higher flow rates, which is governed by the interplay between elongation and restriction of the arc. Indeed, as the flow rate increases, the afterglow temperature decreases. In the model, this is approximated by one temperature profile, based on the available experimental data. The full approach is explained in the ESI (Sections S.1.2, S.2.2.2c and Fig. S.6†). Measuring the temperature in the afterglow with a thermocouple is not possible. Indeed, it resulted in broadening of the plasma effluent, and in plasma arcing onto the thermocouple (see ESI, Fig. S.3†), rendering the measurements invalid.

We would like to note that the methods used for temperature measurements of the plasma arc (OES) and the afterglow (Rayleigh scattering) are complementary: due to geometrical constraints, Rayleigh scattering cannot be applied to study the arc, while OES cannot be used to study the gas temperature in the afterglow due to very low (almost negligible) emission of the afterglow.

Due to the short pulse duration, the time-averaged temperature of the jet never exceeds 390 K. This means that even though on a microscopic the temperature drops from 1750 to

room temperature over 10 mm, on a macroscopic scale this temperature drop is due to the cooling through heat exchange with surrounding cooler gas and is not as substantial (*i.e.*, from approximately from 330–390 K T_{room} = 308 K). This temperature drop agrees well with the literature reports on this phenomenon.[55,56]

The thermal diagnostics provide us sufficient information on the temperature behaviour in the plasma and in the afterglow, allowing to model a large chemistry set without solving for the heat balance in the model itself. This is a justified but considerate simplification to gain more insight into the underlying chemistry while keeping the computational resources feasible. Although not needed in the quasi-1D model, a full heat balance would provide interesting insight. However, it is a topic of a separate study, outside the scope of this work. Just like in the experiments, the model considers only a fraction of the gas being plasma-treated by a pulse train, while the other molecules do not pass through the actual plasma zone. In practice, we have accounted for this by multiplying the calculated reactive plasma species densities by the effective treatment fraction of 3.0%, as estimated from the experiments (for the calculations, see ESI: Section S.2.2.1†).

Results and discussion

NO_x production and energy consumption (EC)

The Soft Jet produces NO and NO_2 at every flow rate investigated (0.4–2.0 L min^{-1}). As the flow rate increases, the NO concentration drops, due to the shorter residence time of the gas in the plasma (Fig. 4; dotted green curve). The NO_2 concentration remains approximately constant, but is considerably lower than the NO concentration at all flow rates. It is known from previous studies of NO_x production in plasma that NO_2 is formed from NO.[14,15] As the equilibrium between NO and NO_2 is reached more quickly than the time needed to initially form NO, the NO/NO_2 ratio is lower at high flow rates (short residence time) compared to low flow rates (long residence time).

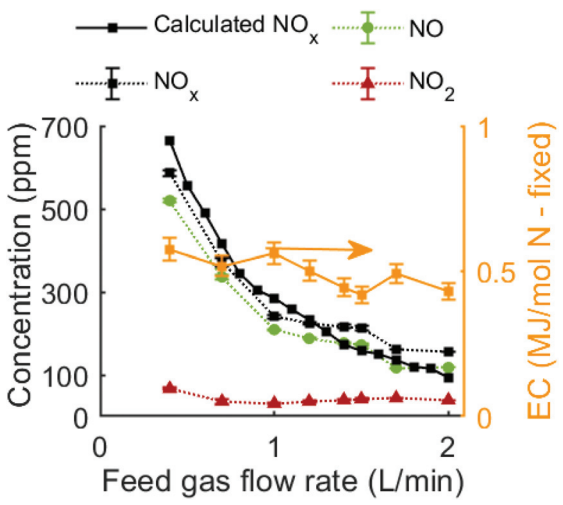

Fig. 4 NO, NO_2 and total NO_x (dashed lines) concentration as measured by FTIR, calculated total NO_x concentration (black; full line) and measured EC (orange; right *y*-axis) as a function of the feed gas flow rate. Error bars are plotted but are barely visible at most flow rates.

The FTIR spectra confirm there is no production of O_3, N_2O_5, N_2O_3, N_2O and NO_3 at the investigated flow rates. In other words, we see a good selectivity towards NO/NO_2, which can be used directly for fertiliser and base chemical production.

The minimum EC in the Soft Jet of 0.42 ± 0.03 MJ $(mol\ N)^{-1}$ is reached at 1.5 L min^{-1}. Indeed, because the concentration stays constant between 1.2 and 1.5 L min^{-1}, even though the residence time is shorter at higher flow rates, a minimum in the EC is reached (Fig. 4; orange curve), corresponding to a maximum NO_x production rate of 28.4 ± 0.4 mg h^{-1} (see ESI: Fig. S.9† for the production rates at all gas feed flow rates). To the best of our knowledge, such a low EC – close to the theoretical minimum EC of 0.2 MJ $(mol\ N)^{-1}$ (*cf.* Introduction) – has never been reported up to now in atmospheric-pressure plasmas. In the next section we discuss these results in the framework of the state of the art.

The calculated NO_x concentration (Fig. 4; full black curve) as a function of flow rate is in good agreement with the experimental data (dotted black curve), both in trend and absolute values. The calculated NO_2 concentration is underestimated (<1 ppm at all investigated flow rates), however rather than tuning the reaction rate constants to account for this underestimation, we prefer using only reliable scientific works that investigated reaction rate constants. Indeed, we do not know what exact (combination of) reaction rate constants might be slightly over- or underestimated, and tuning the rate constants in order to reach a better agreement would therefore not have a strong scientific basis. In any case, we only compare the total NO_x concentration, because the oxidation of NO into NO_2 can still occur after the plasma or in the gas tubing to the FTIR, which is not included in the model.

Finally, just like in the experiments, there is no production of O_3, N_2O_5, N_2O_3, N_2O and NO_3 in the model. This means our model can predict the chemistry of the Soft Jet fairly well, in a wide range of flow rates, and therefore can be used to gain a deeper understanding of the mechanisms that lie at the base of this very energy-efficient NO_x production (see Mechanisms of energy-efficient NO_x production in pulsed plasma section).

Comparison with the state of the art

As mentioned above, to our knowledge the EC obtained in our Soft Jet is by far the lowest value reported in literature for plasma-based NO_x production at atmospheric pressure. The NO_x or NO concentrations and associated EC reported in various plasma types in literature are summarised in Table 2. As mentioned before, microwave plasmas at reduced pressure (0.01–0.07 atm) show the best performance out of all the reported works, in terms of both NO_x concentration and EC.[32,33,57] The EC of microwave plasmas at reduced pressure, however, would be considerably higher if it would also account for the energy required to maintain low pressure and cooling of the reactor, which is not the case. Furthermore, the reduced

Table 2 Overview of the different reported NO_x concentrations and associated EC in various types of plasma reactors in literature. More elaborate discussions on the state of the art of plasma-based NO_x production can be found in the papers of Bogaerts & Neyts,[10] Jardali *et al.*[15] and Rouwenhorst *et al.*[11]

Plasma type	Concentration (%) (products)	EC (MJ (mol N)$^{-1}$)	Ref.
Electric arc (Birkeland–Eyde)	2 (NO)	2.4–3.1	20 and 21
Electric arc with water injection	4.7 (NO)	3.5	58
Exploding water jet discharge	1 (NO_x)	47	26
Spark discharge	— (NO and NO_2)	20.27 and 40	22
Transient spark discharge	— (NO and NO_2)	8.6	23
Pin-to-plane ns-pulsed spark discharge	— (NO and NO_2)	5.0–7.7	27
Pulsed arc discharge	— (NO_x)	10.6	59
Radio-frequency crossed discharge	(HNO_3) (NO and NO_2)	24–108	24
Laser-produced discharge	— (NO and NO_2)	8.9	25
(Positive/negative) DC corona discharge	(NO and NO_2)	1057/1673	22
Pulsed corona discharge	(HNO_3)	186	26
Shielded sliding discharge	0.1 (NO_x)	15.4	60
Pin-to-plane DC glow discharge	(NO and NO_2)	7	27
Pin-to-pin DC glow discharge	0.7 (NO and NO_2)	2.8	28
Dielectric barrier discharge	0.6 (NO and NO_2)	56–140	27
Packed dielectric barrier discharge (γ-Al_2O_3)	0.5 (NO and NO_2)	18	29
DC plasma arc jet	6.5 (NO and NO_2)	3.6	61
Propeller arc	0.4 (NO and NO_2)	4.2	27
Pulsed milli-scale gliding arc	1–2 (NO and NO_2)	2.8–4.8	19 and 36
Gliding arc plasmatron	1.5 (NO and NO_2)	3.6	14
Rotating gliding arc	5.4 (NO and NO_2)	2.5	15
Atmospheric pressure microwave plasma	3.8 (NO_x)	2.0	34
Microwave plasma	0.6 (NO and NO_2)	3.76	30
Microwave plasma with catalyst ($MoCO_3$)[a]	6 (NO)	0.84	57
Pulsed microwave discharge[a]	6 (NO)	0.6	32
Microwave plasma with magnetic field[a]	14 (NO)	0.28	33
Pulsed plasma jet (Soft Jet)	0.02 (NO_x)	0.42	This work

[a] Obtained at reduced pressure (0.01–0.07 atm).

pressure operation makes them also less appealing for industrial exploitation.

The very low EC reached with our Soft Jet shows that values close to the theoretical minimum EC for plasma-based NO_x production at atmospheric pressure can be achieved in practice. Although the Soft Jet as is cannot be used in most applied settings directly, because of the rather low NO_x concentration achieved, the knowledge about the low EC close to the theoretical minimum is highly beneficial, as properties of the Soft Jet that lie at the base of this low EC can be used to inform further research.

Mechanisms of energy-efficient NO_x production in pulsed plasma

In literature, the positive influence of pulsed plasma in N_2 fixation (either due to arc rotation[15,37] or by pulsing the power,[40] like the Soft Jet),[19,27,32,59] has been reported, and to a certain extent their physical characteristics have been studied.[44,62–64] However, because the reported plasma reactors are so different in performance and type, isolating the function of pulsing and determining whether or not and how significantly it enhances the energy efficiency of NO_x formation is challenging. Therefore, the knowledge of pulse-driven chemistry is very limited.[65,66] Our model allows us to elucidate the underlying mechanisms for our pulsed plasma source, which will provide us general insight in the role of pulsing for reaching the most energy-efficient plasma-based NO_x formation.

Conditions for energy-efficient NO_x production. To understand the benefits of pulsing, we first need to clarify the difference between thermal and non-thermal plasmas. In thermal plasmas, the heavy species (gas molecules, radicals, ...) and electrons are in thermal equilibrium (*i.e.*, same temperature), and a large fraction of the input energy (plasma power) is lost to gas heating. The high gas temperature ($T_g \sim 10^4$ K) not only increases the EC, but can also impede effective gas conversion by destroying the products formed.[46] In "warm" (or quasi-thermal) plasmas, the electron temperature (around 1 eV) higher than the temperature of the heavy species, but the latter still can reach several thousands of Kelvin.[11] This electron temperature is ideal for efficient vibrational excitation of N_2 molecules,[10,36] which is the most efficient path for dissociation and for energy-efficient NO_x formation through the vibrationally-enhanced Zeldovich mechanism (see reactions (R1) and (R2) in the Introduction). On the other hand, the relatively high gas temperature reduces the vibrational population by vibrational–translational (V–T) relaxation, *i.e.*, collisions of the vibrational levels with ground state molecules, causing further gas heating.[37,40] Finally, in non-thermal plasmas, the gas temperature remains near room temperature, but the electron temperature is several eV, so the energy put into the plasma is used for gas conversion instead of gas heating.[10] However, the electron temperature is typically too high for efficient vibrational excitation of N_2 molecules.

The holy grail in energy-efficient plasma-based NO_x production is thus to find plasma conditions which generate an

electron temperature around 1 eV. This typically corresponds to a reduced electric field (*i.e.*, ratio of electric field over gas number density; *E*/*N*) up to 50 Td. These conditions are most suitable for N_2 vibrational excitation (see ESI: Fig. S.10†). At the same time, the gas temperature should be kept low, to maintain a high vibrational population of the N_2 molecules. Such conditions are more easily achieved at low pressures, where collisions (including V–T relaxation) are less prominent (see also the best values in Table 2, for low-pressure plasmas). However, by pulsing the plasma power,[23,40,43,44] the same conditions may be reached at higher (*e.g.*, atmospheric) pressure, because the time during the pulses is too short for considerable gas heating.[40] This eliminates the need for low-pressure equipment, which significantly enhances the process cost.[10]

Due to its pulsing regime, our Soft Jet obviously meets the requirements of this holy grail for energy-efficient NO_x production, exactly by the combination of high vibrational excitation and limited gas temperature (strong V–T non-equilibrium; see Introduction). This is clearly revealed from our model. Indeed, the calculated reduced electric field is around 30 Td, resulting in an electron temperature around 0.7–1.0 eV in the pulses, for the various conditions investigated (see Fig. 3b for the condition of 1 L min^{-1} feed gas flow rate. As mentioned above, these values of reduced electric field and electron temperature are ideal for transferring most of the electron energy to N_2 vibrational excitation.[36] In addition, the electron number density is around 10^{13} cm^{-3} during the pulses (see also Fig. 3b), which is fairly high, and thus also beneficial for strong vibrational excitation.

Finally, the gas temperature, while being high (1750 K) during the pulses, reduces to near room temperature in between the pulses (interpulse period; see Fig. 3a), and the time for V–T relaxation during the pulses is too short for significant vibrational depopulation. Hence, a strong V–T non-equilibrium is reached, important for splitting the strong triple bond of N_2: the vibrationally excited N_2 molecules can more easily overcome the energy barrier of NO_x formation through the non-thermal Zeldovich mechanism, as discussed above. The degree of N_2 vibrational excitation will be discussed in next section.

Influence of pulsing on the vibrational excitation of N_2 and O_2. Fig. 5 shows the calculated NO concentration as a function of time, as formed during the train of pulses, within the gas residence time in the plasma (Fig. 5a; black curve), as well as the calculated vibrational distribution function (VDF) of N_2 (Fig. 5b) at the time points indicated in Fig. 5a. The VDF shows how the energy is distributed among the vibrationally excited levels of a molecule, by plotting the relative density of each level (normalised to the ground state).

In case of V–T equilibrium, the VDF exhibits a Boltzmann distribution, dictated by the gas temperature (orange dashed line in Fig. 5b). The calculated N_2 VDF in our Soft Jet, however, clearly deviates from the thermal Boltzmann distribution. As time increases, the VDF builds up to higher populations of the higher vibrational levels (see plateau in Fig. 5b), significantly above the Boltzmann distribution, *i.e.* a strong V–T non-equilibrium is reached. Inside the pulses, due to the relatively high gas temperatures, V–T relaxation will also occur to some extent, but the rate of V–T relaxation drops drastically when the temperature drops after the pulses.[67] This allows for a longer lifetime of the vibrationally excited states and hence a build-up of the V–T non-equilibrium (or plateau formation in the VDF of N_2) over the time of multiple pulses, as clearly illustrated in Fig. 5b.

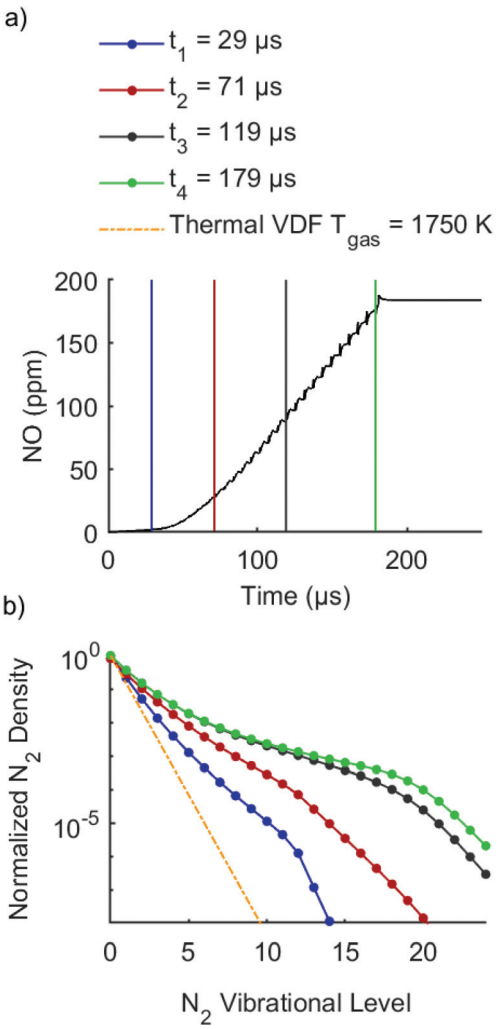

Fig. 5 (a) Calculated NO concentration (black curve) as a function of time, during its residence time in the plasma (at 1 L min^{-1}), encountering a train of pulses, and (b) calculated VDF of N_2 taken in the middle of each pulse, for four different time points, as indicated by the vertical coloured lines in (a). The thermal VDF at 1750 K is also plotted.

Our model reveals that in our Soft Jet on average >99% of NO is formed through vibrationally excited N_2. However, not every vibrational level contributes equally. The exact contribution of each level depends on (i) the energy level (*i.e.*, the higher the level, the more the activation energy for the Zeldovich mechanism is reduced), and (ii) the population density of that level (and as is clear from Fig. 5b, the lower vibrational levels have a higher population density). Fig. 6 shows the contribution of the various N_2 vibrational levels to

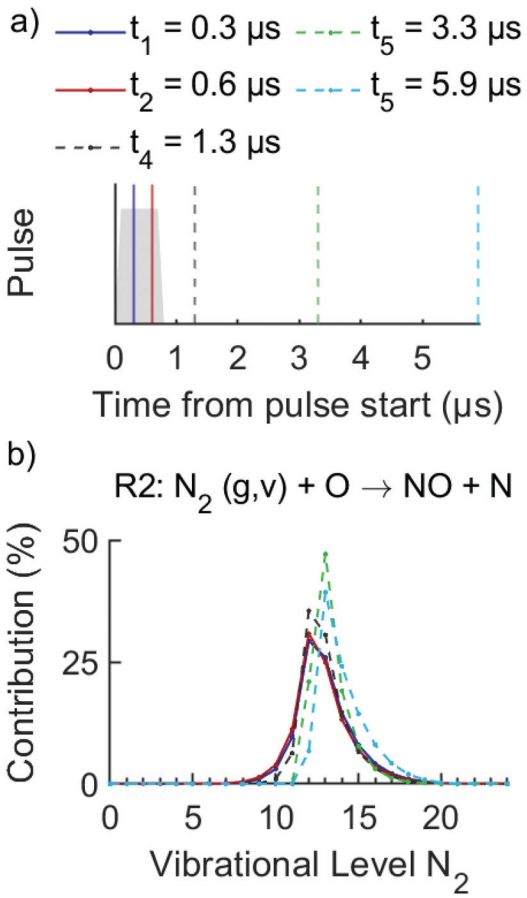

Fig. 6 Contribution of each N_2 vibrational level to the rate of R2 (b), for different time points specified in (a), both during the pulse (solid lines) and during the interpulse time (dashed lines).

the rate of R2, for different times in and after one pulse. $N_2(v_{12})$ has the highest contribution, both during the pulse and the interpulse time. Indeed, the $N_2(v_{12})$ population is sufficiently high (see plateau in the VDF of N_2) and the activation energy is reduced to zero. The densities of the vibrational levels above v_{12} are (significantly) lower, while the lower $N_2(v)$ levels require a higher activation energy for R2.

Note that pulsing is mainly beneficial for increasing the population of $N_2(v)$. Indeed, the V–T relaxation rate constant of O_2 is higher than for N_2 at 300 K ($k_{V\text{–}T\,O_2} = 5 \times 10^{-18}$ cm^3 s^{-1} *vs.* $k_{V\text{–}T\,N_2} = 10^{-18}$–$10^{-19}$ cm^3 s^{-1})[68] and the reaction rate constant for electron impact vibrational excitation of O_2 is lower than for N_2 above electron temperatures of 0.6 eV.[36,68] This results in a Boltzmann-distributed (though elevated) VDF for $O_2(v)$ (see ESI: Fig. S.11†). A lower degree of $O_2(v)$ is, however, not a problem in plasma-based NO_x formation, as the production of O atoms is not the limiting process. Indeed, N_2 has a much higher dissociation energy compared to O_2 (9.79 eV *vs.* 5.15 eV). Our model reveals that the density of O atoms is at least of the same order of magnitude as the density of N atoms (see next section). We should therefore focus especially on the non-equilibrium in the VDF of N_2 instead of O_2.

Interesting to note, even though only a fraction of the gas passes through the arc, this is enough to produce an adequate amount of vibrational population for the formation of NO_x. The model shows how pulsing enables such high vibrational population. A sufficiently high vibrational population (be it Boltzmann or non-Boltzmann distributed), combined with a low treatment fraction is not unique to the Soft Jet, a number of other plasma set-ups produce a significant amount of NO_x while working with a small treatment fraction.[14,15,36]

NO_x formation and loss mechanisms during the pulse and interpulse

The most important formation and loss processes of NO (including oxidation to NO_2), as revealed by our model, are listed in Table 3. Their calculated reaction rates are plotted and discussed in detail in the ESI (Fig. S.12†). Here, we present two sequential pulse–interpulse cycles, as a representative case study to explain the main reaction mechanisms in the pulses and during the interpulse times; depicted in Fig. 7. Panel (a) illustrates the reaction analysis, *i.e.*, the importance of the two steps of the (non-thermal) Zeldovich mechanism (R1 and R2), as a function of time during the pulse and interpulse period. Green represents the forward reaction (net NO production), while black corresponds to the back reaction (net NO loss). Panel (b) shows the corresponding densities of NO, NO_2, N and O in the same time-scale, as calculated in the model.

Our model reveals that the non-thermal Zeldovich mechanism promoted by vibrational excitation is the main mechanism for NO formation (R1 and R2; see Table 3); see detailed analysis in ESI, Section S.3.4.† It should be noted that the reactions with highest rate, overall, are the oxidation of NO to NO_2 (R3 in Table 3) and *vice versa* (R4), which produce a limited amount of NO_2 (<1 ppm at all investigated flow rates).

Table 3 Main reactions for the formation and loss (F, L) of NO. The net reactions (R), as they occur for either NO formation or loss (including oxidation to NO_2), are denoted in bold. Note that R1, R2 and R3 are net formation reactions for NO, while R4 is a net loss reaction

	Reaction	Process	
NO formation	$N + O_2(g,v) \rightarrow NO + O$	F1	
	$O + N_2(g,v) \rightarrow NO + N$	F2	
NO loss	$NO + O \rightarrow O_2 + N$	L1	
	$NO + N \rightarrow N_2 + O$	L2	
NO ↔ NO_2	$NO_2 + O \rightarrow NO + O_2$	F3	
	$NO + O_2 \rightarrow NO_2 + O$	L3	
	$NO_2 + M \rightarrow NO + O + M$	F4	
	$NO + O + M \rightarrow NO_2 + M$	L4	
Net reactions	$\mathbf{N + O_2(g,v) \rightleftharpoons NO + O}$	**R1**	**= F1 – L1**
	$\mathbf{O + N_2(g,v) \rightleftharpoons NO + N}$	**R2**	**= F2 – L2**
	$\mathbf{NO_2 + O \rightleftharpoons NO + O_2}$	**R3**	**= L3 – F3**
	$\mathbf{NO + O + M \rightleftharpoons NO_2 + M}$	**R4**	**= F4 – L4**

(g) and (v) denote the molecules in the ground state *vs.* vibrational levels, respectively. Note that F2 can also occur from electronically excited N_2, but our model reveals that its contribution is only significant at early times (7–11% until *ca.* 35 μs), afterwards its contribution drops to zero (10^{-30}%). M stands for any neutral molecule.

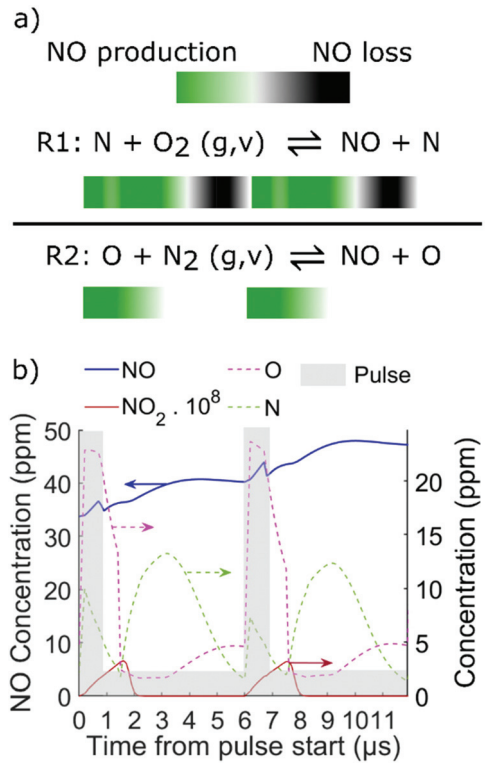

Fig. 7 (a) Importance of R1 and R2 as a function of time during two pulses and interpulse times, as indicated by a gradient scale (green = forward reaction, *i.e.*, net NO production; black = backward reaction, *i.e.*, net NO loss; white = no net production or loss). A darker shade indicates a higher net rate, both in the forward or backward direction. (b) Corresponding concentration of NO, NO_2, N and O for the same two pulses. The NO concentration is shown on the left *y*-axis, while the other species concentrations are shown on the right *y*-axis. Note, the NO_2 concentration has been multiplied by 108 for better visibility.

However, they do not contribute to the initial NO_x formation, and are therefore not shown in Fig. 7.

R1 is mainly important during the pulses, due to the high gas temperature. Its rate rises during successive pulses because more N atoms become available. Thanks to the strong V–T non-equilibrium (see Fig. 5b above), N_2 dissociation is not the limiting step. Indeed, Fig. 7b shows that the N and O concentrations are of the same order of magnitude.

After the pulses, the rate of R1 gradually drops to zero due to the strong temperature drop, which reduces the reaction rate constant (k) with a factor 10^6 (see ESI: Fig. S.13a;† full line). Note, however, that the rate of R1 does not drop below zero (which would correspond to NO loss) during the interpulse time. This is an interesting aspect that will be discussed in more detail in the next section.

The rate of R2 shows roughly the same trend as for R1 during the pulses, due to the high gas temperature. After the pulse, however, the rate rises further, even though the rate coefficient drops due to the lower temperature (see ESI: Fig. S.13b;† full line). This is because N_2(v) builds up a strong V–T non-equilibrium during the interpulse time, and additionally an abundance of O atoms is produced during and right after the pulse (through R1; see dashed pink curve in Fig. 7b). Subsequently, the rate of R2 drops below zero, corresponding to net NO loss. Species availability is the determining factor at this stage. Indeed, during the second half of the interpulse period, less O atoms are available due to the drop in the rate of R1, and the N atoms are now preferably used for the back reaction of R2. Important to note is that the negative rate of R2 never exceeds the positive rate (*i.e.*, production of NO). Hence, while the NO production slows down and the NO concentration drops slightly near the end of the interpulse time, the NO concentration at the end of the pulse–interpulse cycle is still higher than in the beginning of the pulse, demonstrating that the NO concentration gradually builds up as a function of time, as is also clear from Fig. 5a above.

In general we can conclude that the two steps of the non-thermal Zeldovich mechanisms dominate the NO production. They occur at high rates during the pulses, and gradually become negligible (for R1) or occur in the backward direction (for R2) during the interpulse period, but overall, they lead to a steady rise in NO concentration as a function of time.

How pulsing assists N_2 fixation at low energy consumption

We now discuss the specific lessons learned from the above reaction analysis, that can be applied to plasma-based N_2 fixation more in general. Our Soft Jet plasma obviously results in very low EC, and this is clearly attributed to the pulsing.

Exploiting the vibrational–translational non-equilibrium of N_2. The pulse train builds up the N_2(v) population during the pulses *via* electron impact vibrational excitation and vibrational–vibrational (V–V) exchanges between vibrationally excited N_2 and O_2 molecules. At the same time, the temperature drop in between the pulses prevents two things: (1) it prevents loss of vibrational energy caused by V–T relaxation. Indeed, low temperature plasma-based chemistry aims to minimise energy losses through gas heating (hence through V–T relaxation) to maximise the selective input of energy into molecules for chemical reaction though for example vibrational excitation. (2) It prevents N_2–O_2 V–V exchanges. The latter was found to be a limiting mechanism for energy-efficient NO_x production in a gliding arc plasmatron in our previous work.[14] Indeed, because O_2–O_2 V–T relaxation is faster than N_2–N_2 V–T relaxation,[67] the N_2–O_2 V–V exchanges connect the vibrational energy of N_2 to a sink of O_2–O_2 V–T relaxation. However, in our Soft Jet plasma, due to the temperature drop after the pulses, the O_2–O_2 V–T relaxation rate drops and this vibrational sink is limited, hence decreasing the loss of energy into heat that would be caused by V–T relaxation.

If power pulsing is properly adapted in the design of other plasma sources, their EC could also be minimised. In order to use pulsing in the most optimal way, a balance has to be found between pulse-on and pulse-off times and the associated treatment fraction. Indeed, when the pulse is off for a longer time to ensure cooling, the gas can obviously not be treated and will therefore not be converted. The pulse charac-

teristics are clearly the underlying reason for the low EC of our Soft Jet, but the limited treatment fraction is also why the NO_x concentration is low compared to other plasma types. Modelling can help in this regard: by changing the pulse characteristics, an optimum between both should be found.

Suppressing the back reactions of the Zeldovich mechanism. Next to promoting the N_2 vibrational population, the other main challenge in plasma-based NO_x formation is limiting the back reactions of the Zeldovich mechanism (L1 and L2 in Table 3) to prevent NO_x destruction. In continuous plasmas, which operate at constant temperature, this is not straightforward, because both the back and forward reactions are promoted at higher temperatures. However, their temperature dependence is not exactly the same, and we can exploit this in pulsed plasmas, due to the temperature drop in between the pulses. The rate coefficients of the Zeldovich reactions are plotted as a function of the gas temperature in the ESI (Fig. S.13†).

Another point of attention, specifically for the Zeldovich mechanism, is that both forward reactions (F1 and F2) and their back reactions (L1 and L2) compete for the same species. For instance, the O atoms are used for NO formation (F2) and for NO loss (L1). By pulsing the plasma, the temperature dependence of the corresponding reaction rate coefficients can be used to selectively limit the loss reaction (L1). Indeed, the rate coefficients of both the forward and back reaction of R1 increase with temperature, but the temperature dependence for L1 is much more pronounced (see ESI, Fig. S.13a†). Therefore, the drop in temperature in the interpulse period essentially limits the back reaction. In addition, while the rate coefficients of both L1 and F2 are more temperature-dependent than for L2 and F1 (Fig. S.13†), the rate of F2 is significantly enhanced by the rise in $N_2(v)$ population during the interpulse period, and therefore the O atoms are preferable consumed in F2 (NO production) as opposed to L1 (NO loss).

In the case of R2, suppressing the back reaction (L2) is more challenging, as its rate coefficient is temperature-independent and relatively high compared to the other reactions at play in the Zeldovich mechanism (Fig. S.13b†). The rate coefficient of the forward reaction would only be greater than that of the back reaction above 13 200 K. This means that a drop in temperature does not favour one reaction over the other, but instead, it is more a matter of reactive species availability (O and $N_2(g,v)$). Thus, based only on the rate coefficients, R2 would benefit from a high temperature (and not from the temperature drop after the pulses), but it is also strongly promoted by a high $N_2(v)$ population, which is more pronounced at lower temperature. Hence, a balance between these factors needs to be found to fully exploit pulsing in order to maximise energy-efficient NO_x production in plasma.

Economic viability of plasma-based NO_x production

When discussing plasma-based N_2 fixation, the comparison with the HB process is commonly made, based on production rate and EC of N-fixated species. However, the inherent differences between the HB process and plasma-based N_2 fixation are substantial, and plasma-based processes offer other advantages, because they are electricity-based, flexible, and they can operate on a small scale for decentralisation, as explained in the Introduction. Therefore, a direct comparison with the HB process regarding production rate and EC is not a great indicator of whether or not plasma-based N_2 fixation is economically viable.[10] To answer the latter, Rouwenhorst *et al.* performed a techno-economic analysis (TEA) on plasma-based NO_x production,[11] and Anastasopoulou *et al.* carried out a Life Cycle Assessment (LCA) of plasma-based NO production.[69]

The TEA concluded that plasma-based NO_x production for HNO_3 synthesis will become a highly competitive alternative to electrolysis-based HB combined with the Ostwald process, if the EC can be reduced to 0.7 MJ (mol N)$^{-1}$.[11] This is mainly due to the low capital expenditure of plasma-based conversions.[11] The lowest theoretical EC limit of plasma-based NO_x production is 0.2 MJ (mol N)$^{-1}$,[45] while the EC of NH3 synthesis *via* the Haber–Bosch process is at least two times higher (0.48 MJ (mol N)$^{-1}$).[10] This potential is a large driving force in plasma-based NO_x production research.[45] However, in practice such a low EC had not yet been reported in atmospheric-pressure plasmas, before this work.

Likewise, the LCA encourages plasma-based N_2 fixation research by stating that plasma demonstrates strong capabilities in becoming a viable alternative to the current nitric acid production process, provided that certain optimization steps are considered, such as the use of renewable energy and at least either 10% NO yield, tail gas recycle or energy recovery.[69]

Our work demonstrates that plasma-based NO_x production can meet the first prerequisite, based on the TEA, namely an EC below 0.7 MJ (mol N)$^{-1}$. By combining knowledge from a pulsed plasma source, like the Soft Jet, with other well-performing atmospheric pressure plasma setups, such as a rotating gliding arc plasma (5.4% NO_x; 2.5 MJ (mol N)$^{-1}$),[15] we believe it is attainable to meet the second prerequisite, based on the LCA, regarding the NO_x yield as well.

Conclusions

We presented a pulsed power plasma source (Soft Jet) operating at atmospheric pressure with dry air as feed gas, for NO_x production at a very low energy consumption (EC) of 0.42 ± 0.03 MJ (mol N)$^{-1}$. This is the lowest EC reported for plasma-based NO_x production at atmospheric pressure to date.

To gain insight into the underlying mechanisms of this record-low EC, we developed a chemical kinetics model, which provides very good agreement with the experiments at the full range of flow rates (0.4–2.0 L min^{-1}) and can thus be used for reaction analysis. The model pinpoints the specific aspects of pulsed plasma power, that allow for such a low EC.

Our reaction analysis indeed illustrates that pulsing is the key for energy-efficient plasma-based NO_x production, by the drop in gas temperature in between the pulses, which affects the rates of the forward and back reactions of the Zeldovich mechanism in a delicate way, and also enhances the N_2

vibrational population, crucial for the (most efficient) non-thermal Zeldovich mechanism.

The exact pulse and interpulse times appear to be critical for finding a balance between the drop in temperature and the fraction of gas treated by the plasma (pulses). In our Soft Jet, this ratio of pulse and interpulse times appears to be nearly ideal for energy-efficient NO_x formation, as evidenced by the unprecedented low EC, as compared to other studies in literature. On the other hand, the NO_x concentrations obtained are very low (0.02%), attributed to a limited fraction of gas passing through the plasma, and this might also be improved by a somewhat shorter interpulse period.

While this Soft Jet plasma is thus not suitable for practical applications due to the low NO_x production, the concepts revealed in our study will be very useful for other plasma devices, which exhibit a larger fraction of gas passing through the plasma, and which can hopefully be further improved by a careful selection of the pulse and interpulse times, based on the insights obtained in our study.

In terms of economic viability, we demonstrated that it is possible with pulsed plasma to almost reach the theoretical minimum EC of plasma-based NO_x formation, and to meet the required EC (of 0.7 MJ (mol N)$^{-1}$) for plasmas to be competitive with the electrolysis-based HB and Ostwald process for HNO_3 synthesis, as recently defined in a TEA by Rouwenhorst *et al.*[11]

Additionally, when the insights from our work about the influence of pulsed plasma on the EC can be combined with other well-performing atmospheric-pressure plasma setups, such as a rotating gliding arc plasma (5.4% NO_x; 2.5 MJ (mol N)$^{-1}$),[15] we believe it is realistic to meet the second prerequisite (based on a LCA), regarding the NO_x yield as well.

Sustainable generation of reactive nitrogen (like NO_x) is paramount and plasma-based processes are promising in this field, as they are electricity-driven, and can easily be switched on–off, *i.e.* they can easily be coupled to fluctuating renewable electricity, providing grid stabilisation and peak shaving, and they are suitable for small-scale decentralised fertiliser production. In this work, we showed that pulsed plasmas can be the key for such energy-efficient sustainable fertiliser and base chemical production.

Author contributions

The CRediT system for standardised contribution descriptions was used to allocate author contributions. Elise Vervloessem – conceptualization, data curation, formal analysis, investigation, methodology, software, validation, visualization, writing – original draft, writing – review & editing. Yury Gorbanev – conceptualization, methodology, formal analysis, supervision, writing – original draft, writing – review & editing. Anton Nikiforov – conceptualization, investigation, methodology, validation, supervision, writing – review & editing. Nathalie De Geyter – funding acquisition, project administration, resources, supervision, writing – review & editing. Annemie Bogaerts – conceptualization, funding acquisition, project administration, resources, supervision, writing – original draft, writing review & editing.

Conflicts of interest

There are no conflicts to declare.

Funding

This research was supported by the Excellence of Science FWO-FNRS project (NITROPLASM, FWO grant ID GoF9618n, EOS ID 30505023), the European Research Council (ERC) under the European Union's Horizon 2020 research and innovation programme (grant agreement no. 810182 – SCOPE ERC Synergy project), and through long-term structural funding (Methusalem). The calculations were performed using the Turing HPC infrastructure at the CalcUA core facility of the Universiteit Antwerpen (UAntwerpen), a division of the Flemish Supercomputer Center VSC, funded by the Hercules Foundation, the Flemish Government (Department EWI) and the UAntwerpen.

Acknowledgements

We thank E. H. Choi and coworkers from the Plasma Bioscience Research Center (Korea) for providing the Soft Jet plasma source, as well as K. van't Veer and C. Verheyen for the fruitful discussion on the electron loss fraction calculations. The graphical abstract was designed using resources from Flaticon.com.

References

1 B. L. Bodirsky, A. Popp, H. Lotze-campen, J. P. Dietrich, S. Rolinski, A. Biewald, M. Bonsch, F. Humpeno, I. Weindl, C. Schmitz, C. Mu and M. Stevanovic, *Nat. Commun.*, 2014, **5**, 3858.
2 D. F. Herridge, M. B. Peoples and R. M. Boddey, *Plant Soil*, 2008, **311**, 1–18.
3 J. Sun, D. Alam, R. Daiyan, H. Masood, T. Zhang, R. Zhou, P. J. Cullen, E. C. Lovell, A. Jalili and R. Amal, *Energy Environ. Sci.*, 2021, **14**, 865–872.
4 R. M. Nayak-luke, *Energy Environ. Sci.*, 2020, **13**, 2957–2966.
5 G. Hochman, A. S. Goldman, F. A. Felder, J. M. Mayer, J. M. Alexander, P. L. Holland, L. A. Goldman, P. Manocha, Z. Song and S. Aleti, *ACS Sustainable Chem. Eng.*, 2020, **8**, 8938–8948.
6 M. Kamphus, *Nitrogen + Syngas*, 2014, **328**, 48–53.
7 V. Hessel, G. Cravotto, P. Fitzpatrick, B. S. Patil, J. Lang and W. Bonrath, *Chem. Eng. Process.*, 2013, **71**, 19–30.
8 N. Cherkasov, A. O. Ibhadon and P. Fitzpatrick, *Chem. Eng. Process.*, 2015, **90**, 24–33.

9 J. G. Chen, R. M. Crooks, L. C. Seefeldt, K. L. Bren, R. Morris Bullock, M. Y. Darensbourg, P. L. Holland, B. Hoffman, M. J. Janik, A. K. Jones, M. G. Kanatzidis, P. King, K. M. Lancaster, S. V. Lymar, P. Pfromm, W. F. Schneider and R. R. Schrock, *Science*, 2018, **360**, 1–7.

10 A. Bogaerts and E. C. Neyts, *ACS Energy Lett.*, 2018, **3**, 1013–1027.

11 K. H. R. Rouwenhorst, F. Jardali, A. Bogaerts and L. Lefferts, *Energy Environ. Sci.*, 2021, **14**, 2520–2534.

12 L. Hollevoet, F. Jardali, Y. Gorbanev, J. Creel, A. Bogaerts and J. A. Martens, *Angew. Chem., Int. Ed.*, 2020, **59**, 23825–23829.

13 K. H. R. Rouwenhorst, Y. Engelmann, K. Van'T Veer, R. S. Postma, A. Bogaerts and L. Lefferts, *Green Chem.*, 2020, **22**, 6258–6287.

14 E. Vervloessem, M. Aghaei, F. Jardali, N. Hafezkhiabani and A. Bogaerts, *ACS Sustainable Chem. Eng.*, 2020, **8**, 9711–9720.

15 F. Jardali, S. Van Alphen, J. Creel, H. Ahmadi Eshtehardi, M. Axelsson, R. Ingels, R. Snyders and A. Bogaerts, *Green Chem.*, 2021, 1748–1757.

16 J. T. Herron, *Plasma Chem. Plasma Process.*, 2001, **21**, 581–609.

17 Y. Gorbanev, E. Vervloessem, A. Nikiforov and A. Bogaerts, *ACS Sustainable Chem. Eng.*, 2020, **8**, 2996–3004.

18 S. Sun, Q. An, W. Wang, L. Zhang, J. Liu and W. A. Goddard, *J. Mater. Chem. A*, 2017, **5**, 201–209.

19 B. S. Patil, F. J. J. Peeters, G. J. van Rooij, J. A. Medrano, F. Gallucci, J. Lang, Q. Wang and V. Hessel, *AIChE J.*, 2018, **64**, 526–537.

20 K. Birkeland, *Trans. Faraday Soc.*, 1906, **58**, 98–116.

21 S. Eyde, *J. Ind. Eng. Chem.*, 1912, **4**, 771–774.

22 N. Rehbein and V. Cooray, *J. Electrostat.*, 2001, **51–52**, 333–339.

23 K. Hensel, Z. Machala, M. Janda and V. Martis, *Plasma Chem. Plasma Process.*, 2016, **36**, 767–781.

24 M. J. Pavlovich, T. Oni, C. Galieher, B. Curtis, D. S. Clark, Z. Machala and D. B. Graves, *J. Phys. D: Appl. Phys.*, 2014, **47**, 1–10.

25 M. Rahman and V. Cooray, *Opt. Laser Technol.*, 2003, **35**, 543–546.

26 W. Bian, X. Song, J. Shi and X. Yin, *J. Electrostat.*, 2012, **70**, 317–326.

27 X. Pei, D. Gidon, Y. J. Yang, Z. Xiong and D. B. Graves, *Chem. Eng. J.*, 2019, **362**, 217–228.

28 X. Pei, D. Gidon and D. B. Graves, *J. Phys. D: Appl. Phys.*, 2020, **53**, 044002.

29 B. S. Patil, N. Cherkasov, J. Lang, A. O. Ibhadon, V. Hessel and Q. Wang, *Appl. Catal., B*, 2016, **194**, 123–133.

30 T. Kim, S. Song, J. Kim and R. Iwasaki, *Jpn. J. Appl. Phys.*, 2010, **49**, 126201.

31 B. Mutel, O. Dessaux and P. Goudmand, *Rev. Phys. Appl.*, 1984, **19**, 461–464.

32 L. S. Polak, A. A. Ovsiannikov, D. I. Slovetsky and F. B. Vurzel, *Theoretical and Applied Plasma Chemistry*, Nauka (Science), Moscow, 1975.

33 R. I. Asisov, V. K. Givotov, V. D. Rusanov and A. Fridman, *Sov. Phys. High Energy Chem. (Khimia Vysok. Energ.)*, 1980, **14**, 366.

34 S. Kelly and A. Bogaerts, *Joule*, 2021, **5**, 3006–3030.

35 B. S. Patil, J. Rovira Palau, V. Hessel, J. Lang and Q. Wang, *Plasma Chem. Plasma Process.*, 2016, **36**, 241–257.

36 W. Wang, B. Patil, S. Heijkers, V. Hessel and A. Bogaerts, *ChemSusChem*, 2017, **10**, 2110–2157.

37 S. Van Alphen, F. Jardali, J. Creel, G. Trenchev, R. Snyders and A. Bogaerts, *Sustainable Energy Fuels*, 2021, **5**, 1786–1800.

38 J. Krop, E. Krop and I. Pollo, *Chem. Plasma*, 1979, 242–249.

39 I. Muzammil, D. H. Lee, D. K. Dinh, H. Kang, S. A. Roh, Y. Kim, S. Choi, C. Jung and Y. Song, *RSC Adv.*, 2021, **11**, 12729.

40 S. Van Alphen, V. Vermeiren, T. Butterworth, D. C. M. Van Den Bekerom, G. J. Van Rooij and A. Bogaerts, *J. Phys. Chem. C*, 2020, **124**, 1765–1779.

41 P. Shaw, N. Kumar, H. S. Kwak, J. H. Park, H. S. Uhm, A. Bogaerts, E. H. Choi and P. Attri, *Sci. Rep.*, 2018, **8**, 11268.

42 P. Attri, J. Park, J. De Backer, M. Kim, J. Yun, Y. Heo, S. Dewilde, M. Shiratani, E. Ha, W. Lee and A. Bogaerts, *Int. J. Biol. Macromol.*, 2020, **163**, 2405–2414.

43 C. D. Pintassilgo, O. Guaitella and A. Rousseau, *Plasma Sources Sci. Technol.*, 2009, **18**, 025005.

44 A. Lo, A. Cessou, P. Boubert and P. Vervisch, *J. Phys. D: Appl. Phys.*, 2014, **47**, 115201.

45 V. D. Rusanov and A. A. Fridman, *Sov. Phys. Usp.*, 1981, **24**, 447–474.

46 N. Cherkasov, A. O. Ibhadon and P. Fitzpatrick, *Chem. Eng. Process.*, 2015, **90**, 24–33.

47 Y. Gorbanev, R. Soriano, D. O'connell and V. Chechik, *J. Visualized Exp.*, 2016, **2016**, 1–6.

48 S. Liu and M. Neiger, *J. Phys. D: Appl. Phys.*, 2003, **36**, 3144–3150.

49 A. V. Pipa and R. Brandenburg, *Atoms*, 2019, **7**, 2–18.

50 S. Pancheshnyi, B. Eismann, G. J. M. Hagelaar and L. C. Pitchford, *Computer code ZDPlasKin*, University of Toulouse, LAPLACE, CNRS-UPS-INP, Toulouse, France, 2008, http://www.zdplaskin.laplace.univ-tlse.fr.

51 P. J. Bruggeman, N. Sadeghi, D. C. Schram and V. Linss, *Plasma Sources Sci. Technol.*, 2014, **23**, 023001–023033.

52 I. Sremački, M. Gromov, C. Leys, R. Morent, R. Snyders and A. Nikiforov, *Plasma Process. Polym.*, 2020, **17**, 1–12.

53 A. A. Abdelaziz and H. H. Kim, *J. Phys. D: Appl. Phys.*, 2020, **53**, 114001.

54 R. J. Wandell, H. Wang, R. K. M. Bulusu, R. O. Gallan and B. R. Locke, *Plasma Chem. Plasma Process.*, 2019, 643–666.

55 P. Bruggeman and C. Leys, *J. Phys. D: Appl. Phys.*, 2009, **42**, 05001.

56 R. H. Stark, U. Ernst, M. El-Bandrawy and K. H. Schoenbach, in *IEEE Conference Record – Abstracts. 1999 IEEE International Conference on Plasma Science. 26th IEEE International Conference (Cat. No. 99CH36297)*, 1999, p. 117.

57 B. Mutel, O. Dessaux and P. Goudmand, *Rev. Phys. Appl.*, 1984, **19**, 461–464.

58 J. Krop and I. Pollo, *Chemia*, 1981, **678**, 51–59.
59 T. Namihira, S. Katsuki, R. Hackam, H. Akiyama and K. Okamoto, *IEEE Trans. Plasma Sci.*, 2002, **30**, 1993–1998.
60 M. Thiemann, E. Scheibler and K. W. Wiegand, *Ullmann's Encycl. Ind. Chem.*, 2000, vol. 24, pp. 177–223.
61 J. F. Coudert, J. M. Baronnet, J. Rakowitz and P. Fauchais, *Symp. Int. Chim. Plasmas*, 1977.
62 M. Uddi, N. Jiang, I. V. Adamovich and W. R. Lempert, *J. Phys. D: Appl. Phys.*, 2009, **42**, 075205.
63 R. Ono and T. Oda, *Plasma Sources Sci. Technol.*, 2009, **18**, 035006.
64 A. Lo, A. Cessou and P. Vervisch, *J. Phys. D: Appl. Phys.*, 2014, **47**, 115202–115211.
65 M. Šimek and Z. Bonaventura, *J. Phys. D: Appl. Phys.*, 2018, **51**, 504004.
66 N. A. Popov, *Plasma Sources Sci. Technol.*, 2016, **25**, 044003.
67 I. V. Adamovich, S. O. MacHeret, J. W. Rich and C. E. Treanor, *J. Thermophys. Heat Transfer*, 2008, **12**, 57–65.
68 V. D. Rusanov, A. A. Fridman and G. V. Sholin, *Usp. Fiz. Nauk*, 1981, **134**, 449–472.
69 A. Anastasopoulou, S. Butala, J. Lang, V. Hessel and Q. Wang, *Ind. Eng. Chem. Res.*, 2016, **55**, 8141–8153.